ACS Photonics

Article

pubs.acs.org/journal/apchd5

Films with Tunable Graded Refractive Index Consisting of Spontaneously Formed Mesoporous Silica Nanopinnacles

Shin Kitamura,[†] Yosuke Kanno,[‡] Masatoshi Watanabe,[⊥] Masahiko Takahashi,[†] Kazuyuki Kuroda,[‡,§] and Hirokatsu Miyata*[,†]

[†]Frontier Research Center, Canon Inc., 3-30-2 Shimomaruko, Ohta-ku, Tokyo 146-8501, Japan

[‡]Department of Applied Chemistry, Waseda University, 3-4-1 Ohkubo, Shinjuku-ku, Tokyo 169-8555, Japan

[⊥]Nanomaterials R&D Center, Canon Inc., 3-30-2 Shimomaruko, Ohta-ku, Tokyo 146-8501, Japan

[§]Kagami Memorial Research Institute for Materials Science & Technology, Waseda University, 2-8-26 Nishiwaseda, Shinjuku-ku, Tokyo 169-0051, Japan

Supporting Information

ABSTRACT: Coatings with surfaces packed with pointed projections with subwavelength sizes are known as “moth-eye”, whose graded index structure gives superior antireflection (AR) properties with a small dependence on wavelength and incident angle. However, the optical interface between the AR coating and a substrate still causes reflection, unless the refractive index of the coating is matched to that of the substrate. Here, we show a new AR coating with both graded and tunable refractive index, which completely eliminates distinct optical interfaces. The coating is made of a mesoporous silica film, whose surface is spontaneously converted to an assembly of pointed nanostructure by reactive ion etching, and its refractive index is matched universally to that of a substrate by controlled incorporation of titanium dioxide into the mesopores. This AR coating enables universal ultralow reflection on a substrate over the index range from 1.2 to 1.8 and will be applied widely in practical optics.

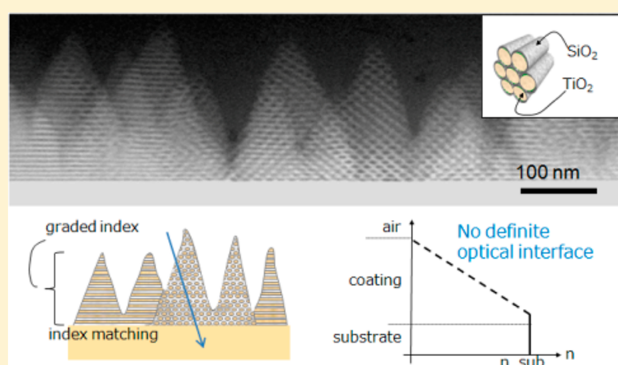

KEYWORDS: *moth-eye, mesoporous, antireflection, index matching, film, subwavelength structure*

Cappadocia in the central Anatolia of Turkey is famous for its characteristic pinnacled rocks, which have been formed by long-term erosion. The formation of such a pinnacled shape by erosion can be downsized to nanometer scales, wherein the erosion is intentionally driven by a chemical reaction during reactive ion etching (RIE).[1−8] Surfaces covered by such subwavelength-scale pinnacles are known as “moth-eye” surfaces[9−12] and are used on various devices such as lenses,[13] light-emitting diodes,[14] photonics sensors,[15] and solar cells[16] using their significant antireflection (AR) effect over a broad spectral bandwidth with a small dependence on the incident angle because of their graded index structure.[1,2,17−19] These moth-eye structures are superior to other types of graded index structures[20] with respect to the continuity of the refractive index change. When these pointed subwavelength structures (SWS) are used for an AR coating of a substrate, the refractive index of the coating needs to be matched to that of the substrate; otherwise, the optical interface between the coating and the substrate causes Fresnel reflection irrespective of the significant suppression of the reflectance at the surface of the AR coating. However, universal fine matching to substrates over a wide range of refractive indices is difficult to achieve because of the restriction of the available materials that allow the formation of the pointed SWS,[10−12] although various methods, including those without a RIE process, have been proposed to form those fine structures.[20−26] In this paper, we report the concept of novel AR coatings based on pointed SWS with tunable refractive indices. The graded index is due to the pointed shape, and the index matching between the coating and the substrate eliminates the reflection at the interfaces of air/coating and coating/substrate, respectively. Consequently, the incident visible light enters the substrate with a given refractive index without meeting any distinct optical interface that causes reflection. Therefore, the configuration of AR reported in this paper provides the ultimate AR coating that can realize “zero reflection”.

The concept of the AR coating in this study is schematically shown in Figure 1. The coating is made of a mesoporous silica (MPS) film with honeycomb-packed cylindrical mesopores, which is prepared by the sol−gel method using a surfactant as a template.[27,28] The surface of the MPS film is spontaneously converted into an assembly of pointed subwavelength structure by an RIE process using a fluorine-containing gas (Figure 1a,

Received: September 13, 2013
Published: November 8, 2013

 © 2013 American Chemical Society

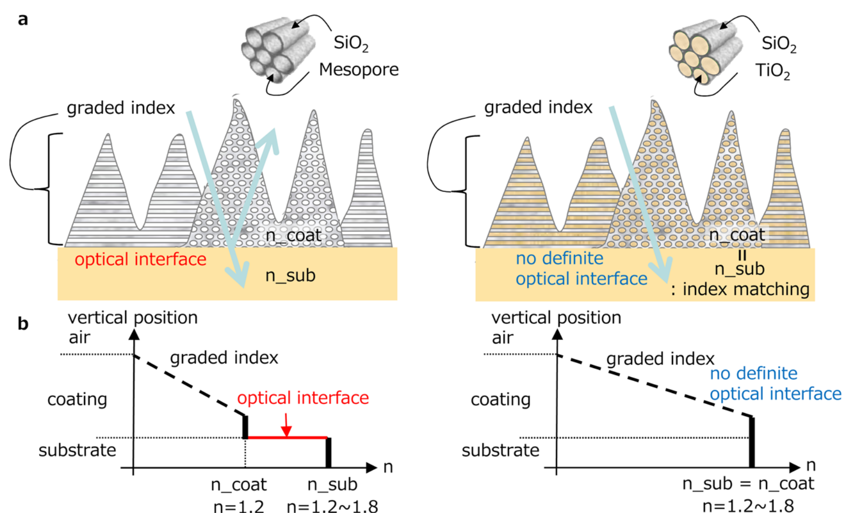

Figure 1. Concept of the AR coating with tunable graded refractive indices. (a) Schematic illustrations of the pointed SWS-MPS films with cylindrical mesopores and (b) the refractive index diagrams of the films before (left) and after (right) the index matching by controlled incorporation of TiO_2. No definite optical interface exists between air and the substrate after the index matching. The notations of n_coat and n_sub represent the refractive index of the SiO_2−TiO_2 composite coating and the substrate, respectively.

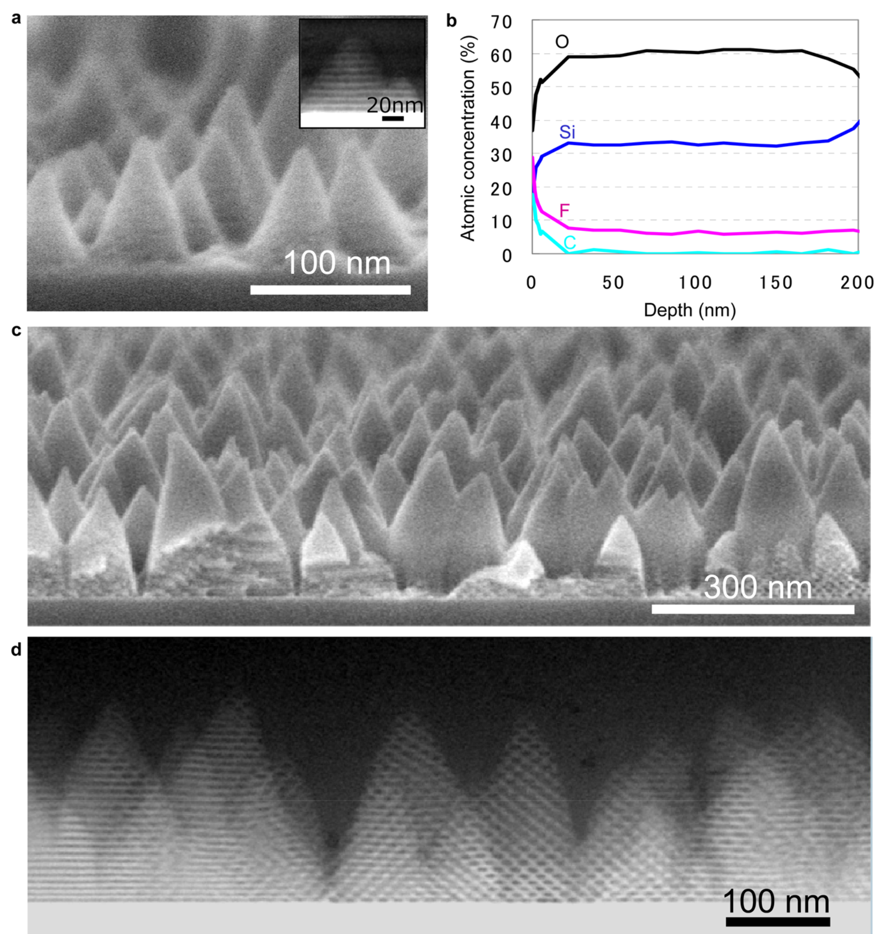

Figure 2. (a) SEM image of the MPS nanopinnacles formed by RIE without pretreatment. Inset: High-resolution HAADF-STEM image. (b) XPS depth profiles of O, Si, F, and C in the MPS film in an early stage of the SWS formation. (c) SEM and (d) high-resolution HAADF-STEM images of the MPS nanopinnacles formed by the RIE after silylation. The scale bars in (a) and (c) are 100 and 300 nm, respectively.

left). This SWS causes the refractive index to change gradually from air to the MPS film (graded index) and eliminates the optical interface between air and the MPS film (Figure 1b, left). The SWS-MPS film undergoes incorporation of a material with high refractive index, titanium dioxide (TiO_2), by low-pressure chemical vapor deposition (LPCVD) to match its refractive index with that of a substrate (Figure 1a right). For the MPS film used in this study with a porosity of 50%, the refractive

dx.doi.org/10.1021/ph400036a | ACS Photonics 2014, 1, 47−52

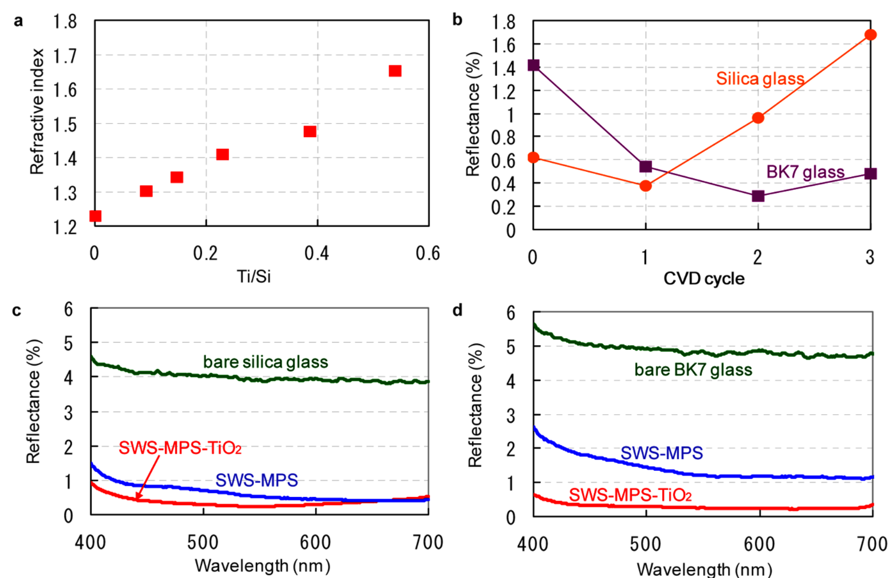

Figure 3. Optical properties of the SWS-MPS AR coatings: (a) relationship between the Ti/Si ratio and the refractive index; (b) dependence of the reflectance (averaged in the range from 400 to 700 nm) on the number of CVD cycles for TiO_2 incorporation; wavelength dependence on the reflectance of (c) silica glass and (d) BK7 substrates with the SWS-MPS.

index can be tuned as desired from 1.2 to 1.8, by varying the filling ratio. After index matching, no abrupt optical interfaces exist anymore on the way from air to the substrate (Figure 1b right). The AR coating in this report with substantially no optical interfaces can suppress the reflection completely on a wide range of substrates with the above refractive index range.

A scanning electron micrograph of the pointed SWS formed by the RIE process is shown in Figure 2a. The surface is packed with submicrometer-scale tiny cones with ~100 nm average height and similar interval. The size and the aspect ratio depend both on the gas species and the conditions of RIE such as power, gas pressure, and bias. The mesopores, which are formed using Pluronic P123 (nonionic surfactant) as a template, completely remain after the SWS formation even at the top and side regions of the cones (Figure 2a inset). The profile of each cone is very smooth, as if it were cut with a sharp knife. With such a morphology, the apparent volume of the MPS continuously increases from top to bottom, which results in an ideal graded refractive index.

The pointed SWS are spontaneously formed without complicated processes for the formation of microscopic masks, which has been indispensable for the formation of such SWS by conventional lithography. Until now, there are no reports on the spontaneous formation of such pointed SWS with silica, presumably because of the high chemical stability of silica. We found that the pointed SWS are specifically formed in mesoporous materials using common etching gases containing fluorine. Apparently, the presence of mosopores is responsible for the formation of the SWS; dense silica is evenly etched under the same conditions. We found that the specificity of MPS for the formation of SWS comes from the uptake of fluorine-containing species into the mesopores and the consequent retardation of etching. Figure 2b shows the depth profiles of the main elements in the MPS film in the course of the SWS formation, recorded by X-ray photoelectron spectroscopy (XPS). It is clearly seen that fluorine is uniformly distributed in the film with a F/Si atomic ratio of ~1/4. In contrast to this, fluorine is detected only at the surface of dense silica, which is smoothly etched by the same RIE process (Supporting Information Figure S1). It is most likely that the reaction products of the RIE process are incorporated into the mesopores and form aggregates, which cause the retardation of the etching rate. This proposed mechanism is supported by the fact that the SWS formation as well as the uptake of fluorine does not take place when the MPS film is heated to 200 °C during the RIE process to suppress the deposition of reaction products (Supporting Information Figure S2).

The proposed formation model, which involves the uptake and the subsequent aggregation of fluorine-containing compounds in the mesopores, suggests that the morphology of the SWS-MPS can be modified by changing the surface energy of the MPS film, which should influence the aggregation behavior. On the basis of this idea, we modified the surface of the MPS film by silylation before the RIE process. The SWS-MPS formed after the silylation with chlorotrimethylsilane consists of cones with much larger aspect ratio, as shown in Figure 2c. This is quite reasonable because lowering of the surface energy should hasten the migration of the deposited species and consequently increase the aggregation, which enhances the resistance to RIE, to increase the aspect ratio. The average height of the cones increases to ~300 nm, keeping the ~100 nm intervals. It is confirmed that the SWS-MPS entirely consists of mesoporous silica (Figure 2d). This SWS with improved height and aspect ratio results in a sufficient graded index for high antireflection performance. The graded index structure of SWS-MPS can eliminate the optical interface between air and the MPS film. However, as described before, reflection takes place at the interface between the MPS and the substrate because of the extremely small refractive index of MPS. In the AR coating in this study, this optical interface can also be eliminated by the precisely controlled incorporation of TiO_2 (n = 2.2 @550 nm)[29] into the mesopores and the consequent matching of the refractive indices of the two.

We incorporated TiO_2 by LPCVD using titanium tetraisopropoxide (TTIP) as a titanium source. This developed process is based on the surface sol–gel chemistry,[30] which enables the deposition of an oxide layer with a precision of a monolayer. In this process, TTIP and water vapor are

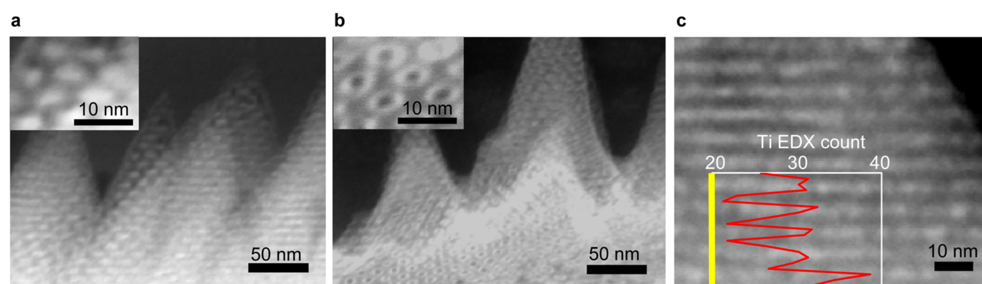

Figure 4. Cross-sectional HAADF-STEM images of the SWS-MPS after (a) four and (b) two cycles of CVD for TiO_2 incorporation. Insets: High-magnification images. (c) High-magnification image of the MPS-SWS after four cycles of CVD and the superimposed Ti profile recorded by STEM-EDX analysis.

alternatively introduced into a chamber, in which the SWS-MPS is placed. This procedure achieves uniform introduction of TiO_2, and the amount of the incorporated TiO_2 can be controlled by the number of cycles of CVD (Supporting Information Figure S3). A linear relationship between the amount of the incorporated TiO_2 (Ti/Si ratio) and the refractive index is confirmed, as shown in Figure 3a. This is taken from a continuous MPS film with a flat surface because refractive indices of the films cannot be measured by ellipsometry after the formation of the SWS. It is shown that the refractive index of the flat MPS film can be tuned in the range from 1.2 to 1.7 by controlling the TiO_2 loading into the mesopores. The porosity of the film is estimated to be ~50% from the refractive index of the hollow MPS film (1.2), by assuming the refractive index of the silica walls is equal to that of dense silica glass, 1.46. With this porosity, the available maximum refractive index is estimated to be ~1.8, when all the mesopores are entirely filled with TiO_2. It is likely that the film with the maximum refractive index and Ti/Si ratio in Figure 3a has not been completely filled with TiO_2 because of problems of the continuous MPS film with complete filling by diffusion. Although the refractive index of the MPS film cannot be measured by ellipsometry after the formation of the SWS, we can estimate it from the Ti/Si ratio obtained by an elemental analysis. After the SWS formation, the incorporation of TiO_2 is much less affected by diffusion of TTIP, because the required diffusion length is drastically reduced. Therefore, we can control the TiO_2 loading simply by the number of CVD cycles up to complete filling.

We formed the SWS-MPS on two kinds of glass substrates, silica glass (n = 1.46) and BK7 (n = 1.52), and incorporated TiO_2 to reduce the reflection by matching the refractive index. The number of CVD cycles for obtaining the lowest reflectance is one and two for silica glass and BK7, respectively, as shown in Figure 3b. For both substrates, excess loading makes the refractive index of the SWS-MPS larger than that of the substrates, which increases the reflectance again. Thus, fine index matching by the optimized cycle of the CVD process is demonstrated on plural substrates with different refractive indices. Even lower reflectance could be achieved by finer control of loading by changing the pressure of TTIP or the temperature during the CVD process.

The reflectance profiles on the two substrates with respective index-matched SWS-MPSs in the visible spectral range (400–700 nm) are shown in Figure 3c and d. It is clearly shown that the reflectance on the two substrates is drastically suppressed. The effect of index matching is remarkable especially on BK7, with a higher refractive index. The reflectance is still larger than 1% when the substrate is coated with a hollow SWS-MPS, although the graded index prevents the reflection at the air/MPS interface.

As described above, the concept of the AR coating has been proven, but we still need to confirm the retention of the original shape of SWS-MPS and the selective deposition of TiO_2 in the mesopores. A high-resolution scanning transmission electron microscopy (STEM) image in a high-angle annular dark field (HAADF) mode recorded for the SWS-MPS after the full TiO_2 incorporation is shown in Figure 4a. In the image, the positions of the mesopores appear brighter than the pore walls. This proves that the pores of MPS are filled with TiO_2 because the contrast of the STEM-HAADF signal is proportional to the square of the atomic number. Thus, the incorporation of TiO_2 into the mesopores without changing the shape of the nanopinnacles is directly confirmed. It is likely that TiO_2 is initially formed on the walls of the mesopores as a uniform layer, and the thickness grows with the CVD cycle to eventually block the mesopores. This is evidenced by the comparison of the images with a smaller TiO_2 loading (Figure 4b), in which the existence of hollow pores is still seen. This layer-by-layer formation of TiO_2 on the wall of the MPS is advantageous for improving the uniformity. The line scan profile of Ti shows complete correspondence of the Ti signal with the period of the mesostructure (Figure 4c). This proves the selective incorporation of TiO_2 into the mesopores.

In general, the moth-eye-type AR coatings have small incident-angle dependence. It is reported that the angle dependence is influenced by the packing and the shape of the projections, and close-packed nanocones allow very low reflectance over a wide range of incident angles.[31] Because the projections of the AR coatings in this paper are closely packed and each shape resembles a cone, the AR coating in this report should have high potential for wide-angle optics. "Zero" reflectance over a wide angle region will truly be realized by the improvement of the controllability of the shape of the nanopinnacles.

In summary, we have demonstrated a novel AR coating, which enables "zero reflection" on substrates with a wide refractive index range, by completely eliminating definite optical interfaces. The superior AR is achieved by the combination of graded refractive index at the surface and index matching at the coating/substrate interface. Such a unique structure is realized by spontaneous formation of pointed subwavelength structures on the surface of a mesoporous silica film and the subsequent controlled incorporation of TiO_2 into the mesopores. The AR coating in this study will widely be applied in practical optics such as lenses, wherein light impinges on a transparent medium from air, because of the advantages in superior performance and facile fabrication.

METHODS

Preparation of MPS Films. The MPS films were formed on a substrate (Si wafer, silica glass, BK7) by dip-coating using a poly-(ethylene oxide)$_{20}$-*b*-poly(propylene oxide)$_{70}$-*b*-poly-(ethylene oxide)$_{20}$ triblock copolymer (Pluronic P123, BASF) as a structure-directing agent. The precursor solution was prepared by adding tetraethoxysilane (TEOS) in an ethanolic solution of P123 containing hydrochloric acid (HCl) and water followed by aging at 25 °C for 3 h. The final molar ratio was TEOS:P123:HCl:H_2O:ETOH = 1.0: 0.0095:0.0011:6.0:8.7. The dip-coating was conducted under an atmosphere of 25 °C, 40% RH, with a withdrawal speed of 1.5 mm/s. The films were subsequently dried in the same atmosphere over 16 h and then calcined, to remove the surfactant, at 400 °C for 4 h in air.

RIE for the SWS Formation. The RIE was performed with a RIE-101ipH (Samco Instruments) using C_3F_8 as an etching gas at a flow rate of 20 SCCM (3 Pa). The RF power and the bias power were set to 500 W and 50 W, respectively. The etching time was set to 90 s.

LPCVD Process for the Incorporation of TiO_2. The MPS films were placed in a stainless chamber, and it was evacuated to 1×10^{-6} Pa. Then TTIP was introduced into the chamber, passing over the sample for 2 h at room temperature. The sample was then evacuated under vacuum (10^{-6}Pa) and finally hydrolyzed at room temperature in air.

Characterization. The morphologies of the MPS-SWS were characterized using a Hitachi S-5500 high-resolution scanning electron microscope at a low accelerating voltage of 2.0 kV. Cross-sectional STEM images were recorded on a Tecnai F30 at an accelerating voltage of 300 kV in HAADF mode, and the distributions of Ti and Si in the images were recorded by energy-dispersive X-ray spectroscopy (EDX) using a silicon solid-state detector. Depth profiles of the elements were recorded by XPS using a PHI Quantera II (ULVAC-PHI) equipped with an Ar ion gun. Reflectance was measured with a SGRM200 (SIGMA-KOKI) in the range from 400 to 700 nm.

ASSOCIATED CONTENT

Supporting Information

SEM image and XPS depth profiles of the main elements in the dense silica film after the RIE process; SEM images and XPS depth profiles of the SWS-MPS prepared at different temperature during RIE; profiles of Ti/Si ratio in the flat MPS films after different numbers of CVD cycles for the incorporation of TiO_2. This material is available free of charge via the Internet at http://pubs.acs.org.

AUTHOR INFORMATION

Corresponding Author

*E-mail: miyata.hirokatsu@canon.co.jp.

Notes

The authors declare no competing financial interest.

ACKNOWLEDGMENTS

The authors acknowledge Dr. O. Albrecht for careful review of the manuscript. The authors thank Dr. W. Kubo for preparation of the film samples.

REFERENCES

(1) Huang, Y.-F.; Chattopadhyay, S.; Jen, Y.-J.; Peng, C.-Y.; Liu, T.-A.; Hsu, Y.-K.; Pan, C.-L.; Lo, H.-C.; Hsu, C.-H.; Chang, Y.-H.; et al. Improved broadband and quasi-omnidirectional anti-reflection properties with biomimetic silicon nanostructures. *Nat. Nanotechnol.* **2007**, *2*, 770–774.

(2) Park, K.-C.; Choi, H. J.; Chang, C.-H.; Cohen, R. E.; Mckinley, G. H.; Barbastathis, G. Nanotextured silica surfaces with robust superhydrophobicity and omnidirectional broadband supertransmissivity. *ACS Nano* **2012**, *6*, 3789–3799.

(3) Jansen, H.; De Boer, M.; Legenberg, R.; Elwenspoek, M. The black silicon method: a universal method for determining the parameter setting of a fluorine-based reactive ion etcher in deep silicon trench etching with profile control. *J. Micromech. Microeng.* **1995**, *5*, 115–120.

(4) Kanamori, Y.; Sasaki, M.; Hane, K. Broadband antireflection gratings fabricated upon silicon substrates. *Opt. Lett.* **1999**, *24*, 1422–1424.

(5) Toyota, H.; Takahara, K.; Okano, M.; Yotsuya, T.; Kikuta, H. Fabrication of microcone array for antireflection structured surface using metal dotted pattern. *Jpn. J. Appl. Phys.* **2001**, *40*, 747–749.

(6) Li, Y.; Zang, J.; Zhu, S.; Dong, H.; Jia, F.; Wang, Z.; Sun, Z.; Zhang, L.; Li, Y.; Li, H.; et al. Biomimetic surfaces for high-performance optics. *Adv. Mater.* **2009**, *21*, 4731–4734.

(7) Sainiemi, L.; Jokinen, V.; Shah, A.; Shpak, M.; Aura, S.; Suvanto, P.; Franssila, S. Non-reflecting silicon and polymer surfaces by plasma etching and replication. *Adv. Mater.* **2011**, *23*, 122–126.

(8) Hsu, C.-H.; Lo, H.-C.; Chen, C.-F.; Wu, C. T.; Hwang, J.-S.; Das, D.; Tsai, J.; Chen, Li.-C.; Chen, K.-S. Generally applicable self-masked dry etching technique for nanotip array fabrication. *Nano Lett.* **2004**, *4*, 471–475.

(9) Bernhard, C. G. Structural and functional adaptations in a visual system. *Endeavour* **1967**, *26*, 79–84.

(10) Li, Y.; Zhang, J.; Yang, B. Antireflective surfaces based on biomimetic nanopillared arrays. *Nano Today* **2010**, *5*, 117–127.

(11) Chattopadhyay, S.; Huang, Y. F.; Jen, Y. J.; Ganguly, A.; Chen, K. H.; Chen, L. C. Anti-reflecting and photonic nanostructures. *Mater. Sci. Eng. R* **2010**, *69*, 1–35.

(12) Brunner, R.; Sandfuchs, O.; Pacholski, C.; Morhard, C.; Spatz, J. Lessons from nature: biomimetic subwavelength structures for high-performance optics. *Laser Photonics Rev.* **2012**, *6*, 641–659.

(13) Disch, A.; Mick, J.; Blasi, B.; Muller, C. Nanostructures on microstructured surfaces. *Microsyst. Technol.* **2007**, *13*, 483–486.

(14) Song, Y. M.; Park, G. C.; Jang, S. J.; Ha, J. H.; Yu, J. S.; Lee, Y. T. Multifunctional light escaping architecture inspired by compound eye surface structures: From understanding to experimental demonstration. *Opt. Express.* **2011**, *19*, 157–165.

(15) Lee, C.; Bae, S. Y.; Mobasser, S.; Manohara, H. A novel silicon nanotips antireflection surface for the micro sun sensor. *Nano Lett.* **2005**, *5*, 2438–2442.

(16) Zhu, J.; Hsu, C. M.; Yu, Z.; Fan, S.; Cui, Y. Nanodome solar cells with efficient light management and self-cleaning. *Nano Lett.* **2010**, *10*, 1979–1984.

(17) Clapham, P. B.; Hutley, M. C. Reduction of lens reflection by moth eye principle. *Nature* **1973**, *244*, 281–282.

(18) Wilson, S. J.; Hutley, M. C. The optical-properties of moth eye antireflection surfaces. *Opt. Acta* **1982**, *29*, 993–1009.

(19) Stavenga, D. G.; Foletti, S.; Palasantzas, G.; Arikawa, K. Light on the moth-eye corneal nipple array of butterflies. *Proc. R. Soc. B* **2006**, *273*, 661–667.

(20) Xi, J. Q.; Schubert, M. F.; Kim, J. K.; Schubert, E. F.; Chen, M.; Lin, S.-Y.; Liu, W.; Smart, J. A. Optical thin-film materials with low refractive index for broadband elimination of Fresnel reflection. *Nat. Photonics* **2007**, *1*, 176–179.

(21) Yamaguchi, N.; Tadanaga, K. Anti-reflective coatings of flowerlike alumina on various glass substrates by the sol–gel process with the hot water treatment. *J. Sol-Gel Sci. Technol.* **2005**, *33*, 117–120.

(22) Okuno, T. Development of subwavelength structure coating (SWC) and its application to imaging lenses. *Proc. SPIE* **2010**, *7652*, 765203–765208.

(23) Lee, Y. J.; Ruby, D. S.; Peters, D. W.; Mckenzie, B. B.; Hsu, J. W. P. ZnO nanostructures as efficient antireflection layers in solar cells. *Nano Lett.* **2008**, *8*, 1501−1505.
(24) Diedenhofen, S. L.; Vecchi, G.; Algra, E.; Hartsuiker, A.; Muskens, O. L.; Immink, G.; Bakkers, E. P. A. M.; Vos, W. L.; Rivas, J. G. Broad-band and omnidirectional antireflection coatings based on semiconductor nanorods. *Adv. Mater.* **2009**, *21*, 1−6.
(25) Ting, C. J.; Huang, M. C.; Tsai, H. Y.; Chou, C. P.; Fu, C. C. Low cost fabrication of the large-area anti-reflection films from polymer by nanoimprint/hot-embossing technology. *Nanotechnology* **2008**, *19*, 205301.
(26) Min, W. L.; Jiang, B.; Jiang, P. Bioinspired self-cleaning antireflection coatings. *Adv. Mater.* **2008**, *20*, 3914−3918.
(27) Alberius, P. C. A.; Frindell, K. L.; Hayward, R. C.; Kramer, E. J.; Stucky, G. D.; Chmelka, B. F. General predictive syntheses of cubic, hexagonal, and lamellar silica and titania mesostructured thin films. *Chem. Mater.* **2002**, *14*, 3284−3294.
(28) Sanchez, C.; Boissiere, C.; Grosso, D.; Laberty, C.; Nicole, L. Design, synthesis, and properties of inorganic and hybrid thin films having periodically organized nanoporosity. *Chem. Mater.* **2008**, *20*, 682−737.
(29) Lien, S.-Y.; Wuu, D.-S.; Yeh, W.-C.; Liu, J.-C. Tri-layer antireflection coatings ($SiO_2/SiO_2-TiO_2/TiO_2$) for silicon solar cells using a sol−gel technique. *Sol. Energy Mater. Sol. Cells* **2006**, *90*, 2710−2719.
(30) Ichinose, I.; Senzu, H.; Kunitake, T. Surface sol−gel process of TiO_2 and other metal oxide films with molecular precision. *Chem. Mater.* **1997**, *9*, 1296−1298.
(31) Chuang, S.-Y.; Chen, H.-L.; Shieh, J.; Lin, C.-H.; Cheng, C.-C.; Liu, H.-W.; Yu, C.-C. Nanoscale of biomimetic moth eye structures exhibiting inverse polarization phenomena at the Brewster angle. *Nanoscale* **2010**, *2*, 799−805.